LA-UR-03-5396, Journal of Sound and Vibration, ***286****(1), 229-250, 2005*

An Outlier Analysis Framework for Impedance-based Structural Health Monitoring

Gyuhae Park*, Amanda C. Rutherford, Hoon Sohn, Charles R. Farrar

Engineering Sciences & Applications Division
Los Alamos National Laboratory
Los Alamos, NM 87545

ABSTRACT

This paper presents the use of statistically rigorous algorithms combined with active-sensing impedance methods for damage identification in engineering systems. In particular, we propose to use statistical pattern recognition methods to address damage classification and data mining issues associated with the examination of large numbers of impedance signals for health monitoring applications.

In this paper, in order to diagnose damage with statistical confidence, the impedance-based monitoring is cast in the context of an outlier detection framework. A modified auto-regressive model with exogenous inputs (ARX) in the frequency domain is developed and the damage sensitive feature is obtained by quantifying the differences between the measured impedance and the output of the ARX model. Furthermore, because of the non-Gaussian nature of the feature distribution tails, extreme value statistics (EVS) is employed to develop a robust damage classifier. This paper concludes with a numerical example on a 5 degree-of-freedom system and an experimental investigation on a multi-story building model to demonstrate the performance of the proposed concept.

* Author to whom correspondence should be addressed. Email:gpark@lanl.gov

1. Introduction

Damage identification is an area of interest in many engineering industries and is the most fundamental part of structural health monitoring and damage prognosis problems. The process of implementing a damage detection strategy can be best addressed as a problem in statistical pattern recognition [1]. In this context, the damage detection and structural health monitoring can be broken down into four categories: (1) Operational Evaluation, (2) Data Acquisition and Cleansing, (3) Feature Extraction and Data Compression, and (4) Statistical Model Development. A general overview of this statistical pattern recognition technology can be found in Farrar et al. [2]. The focus of this paper is to address the issues associated with categories (3) and (4) coupled with the use of the impedance-based structural health monitoring techniques. In the process of the feature extraction, data measured from the system or structure are converted into a key information that can be used to identify whether damage has occurred or not in a structure. This information is referred to as a damage sensitive feature. The feature extraction usually involves the condensation of large amount of available data into a much smaller data set that can be analyzed in a statistical manner.

Impedance-based structural health monitoring has shown promising successes in monitoring and finding minor changes in structural integrity [3,4]. The basic concept of the method is to use high frequency structural excitations to monitor the local area of a structure for changes in structural impedance that would indicate imminent damage. By employing high frequency ranges (> 30 kHz), the method is very sensitive to incipient changes in structural integrity. Another key aspect of the impedance method is the use of piezoelectric (PZT) materials as a collocated sensors and actuators. The use of

collocated, self-sensing actuators provides a solution to the common structural health monitoring problem of "how to excite a structure" and considerably reduces hardware complexity and power requirement. Furthermore, the small, non-intrusive PZT can be easily installed into and used to monitor remote, inaccessible locations.

In order for the impedance method to mature from laboratory demonstration problems to field implementation on complex structures, statistically rigorous algorithms need to be employed to assess the variation of the signature patterns caused by structural damage. However, the signal processing part of the impedance method is probably the least explored area to date. Impedance-based health monitoring is still heavily based on variation of impedance response. Damage metric charts (described in the next section) are used only when a qualitative comparison between data sets needs to be made. Because the impedance-based method primarily relies on experimental data with difficulties in modeling at such high frequency ranges, the use of statistical analysis procedures is required if changes in the impedance caused by structural damage are to be distinguished from those caused by operational and environmental variability.

In this paper, the impedance-based monitoring is cast in the context of an outlier detection framework. A modified auto-regressive model with exogenous inputs (ARX) in the frequency domain is developed. The damage sensitive feature is then computed by differentiating the measured impedance and the output of the ARX model. Because of the non-Gaussian nature of the extracted features, extreme value statistics (EVS) is employed to develop a robust damage classifier.

In the following sections, the theoretical explanation of the techniques is presented and then, the theory is tested on a numerical example of a 5 degree-of-freedom system and an experimental model of a three story steel frame building.

2. Impedance-based Structural Health Monitoring

The impedance-based health monitoring method utilizes the direct as well as the converse piezoelectric effect simultaneously. Hence, one PZT patch can be used for both actuation and sensing of the structural response. The PZT is normally bonded directly to the surface of the structure. The force transmission between the bonded PZT and the structure can be modified by the bond layer, therefore, the use of high-strength adhesives is required to ensure a better mechanical interaction. By analyzing the interaction of the PZT with the host structure, it has been shown that the electrical impedance of PZT is directly related to the mechanical point impedance of the external structure, as shown in the following equation [5],

$$Y(\omega) = \frac{I}{V} = i\omega a \left(\bar{\varepsilon}_{33}^{\ T} - \frac{Z\ (\omega)}{Z\ (\omega) + Z_a(\omega)} d_{3x}^2 \hat{Y}_{xx}^{\ E} \right) \tag{1}$$

where Y is the electrical admittance (inverse of impedance) of the PZT, Z_a and Z are the mechanical impedances of the PZT material and structure, respectively V is the input voltage to the PZT actuator, and I is the output current from the PZT, a, d_{3x}, Y_{xx}^{E}, $\bar{\varepsilon}_{33}^{\ T}$ are the geometry constant, piezoelectric coupling constant, Young's modulus, and complex dielectric constant of the PZT at zero stress, respectively.

Equation (1) sets the groundwork for using PZTs for impedance-based structural health monitoring applications. Assuming that the intrinsic properties of the PZT do not change over the monitoring period of the host structure, Equation (1) clearly shows that the electrical impedance of the PZT is directly related to the mechanical impedance of the host structure. This relationship between electrical and mechanical impedances allows the monitoring of the host structure's mechanical properties using the measured electrical impedance. Consequently, any changes in the electrical impedance signature can be considered as changes in the structural integrity. In order to ensure high sensitivity to incipient damage, the electrical impedance is measured at high frequency ranges. To sense incipient-type damage which does not result in any measurable change in the structure's global stiffness properties, it is necessary for the wavelength of excitation to be smaller than the characteristic length of the damage to be detected [6]. Hence, the frequency range typically used in this technique is in the range of 20 kHz to 250 kHz. At such high frequencies, the wavelength of the excitation is small and is sensitive enough to detect minor changes in the structural integrity. In addition, by using the self-sensing actuation concept and local excitations, the impedance method requires very low voltage (less than 1 volt) compared to those of using separate sensors/actuators. This low voltage level is much more in line with micro-level actuators than the voltages and excitation forces required by competing modal-based diagnostic methods.

An experimental modal test using the electrical impedance of PZT patches (as co-located actuators and sensors) was also investigated by Sun *et al*. [7]. In this paper, the authors discuss that both the point frequency response functions (FRF) of a single location and the transfer FRF between two locations on a structure can be obtained by

measured electrical impedance. This work provides a critical insight into impedance-based structural health monitoring technique, showing that the electrical impedance of a PZT, which can be analogous to frequency response functions, constitutes a unique signature of the dynamic behavior of the structure.

Experimental implementation of the impedance method has been successfully demonstrated on several complex structures. A more complete description of the technique and recent trends in experimental investigations are summarized in the references[3,4].

Quantitative damage assessment with the impedance method is traditionally accomplished through the use of a scalar damage metric. In earlier work [8], a simple statistical algorithm, which is based on frequency-by-frequency comparison and referred to as 'Root Mean Square Deviation' (RMSD) has been used,

$$M = \sum_{i=1}^{n} \sqrt{\frac{\left[\mathrm{Re}(Z_{i,1}) - \mathrm{Re}(Z_{i,2})\right]^2}{\left[\mathrm{Re}(Z_{i,1})\right]^2}} \qquad (2)$$

where M represents the damage metric, $Z_{i,1}$ is the impedance of the PZT measured at healthy conditions, and $Z_{i,2}$ is the impedance for the comparison with the baseline measurement at frequency interval i. In a RMSD damage metric chart, the greater numerical value of the metric, the larger the difference between the baseline and the impedance measurement, indicating the presence of damage in a structure. Raju et al. [9] adopt another scalar damage metric, referred to as the 'Cross-Correlation' metric, which can be used to interpret and quantify information from different data sets. The correlation coefficient between two data sets determines the relationship between two impedance signatures, and provides a qualitative metric chart. In most cases, the results

with the correlation metric are consistent with those of RMSD, in which the metric values increase when there is an increase in severity of damage. Zagrai and Giurgiutiu [10] investigate several statistics-based damage metrics, including RMSD, mean absolute percentage deviation, covariance change, and correlation coefficient deviation. It has been found that the third power of the correlation coefficient deviation, $(1-R^2)^3$, is the most successful damage indicator, which tends to linearly decrease as the crack in a thin plate moves away from the sensor. However, the main limitation of the use of these damage metrics is how to set appropriate decision limits or thresholds values, forming a motivation of this study.

3. Damage Diagnosis by Statistical process control and extreme value statistics

In order to assess damage with statistical confidence and to address the data mining involved in examining large numbers of impedance signals, we investigate the use of statistical process control [11] in an unsupervised learning mode, which is the first step of damage identification. In particular, the statistical process control paradigm developed for vibration measurements by Sohn and Farrar [1] has been extended and applied to the impedance-based methodology.

The developed statistical process control consists of a two-stage prediction model, that is a combination of an auto-regressive (AR) model and auto-regressive model with exogenous inputs (ARX). In a traditional time-series application, an AR-ARX model attempts to predict response at the current time point based on its own past time point responses, as well as the current and past inputs to the system [12]. Residual errors, which quantify the difference between the prediction from the AR-ARX model and the

actual measured time history at each time interval, are then computed and used as a damage sensitive feature [1,13,14]. First, each AR models is constructed with the measured time histories from both undamaged and "in-question" condition as in Equation (3),

$$x(t) = \sum_{j=1}^{p} \phi_j x(t-j) + e_x(t) \tag{3}$$

where *x(t)* donates a known time signal, *p* is an order of the AR model, ϕ_j is a AR coefficient, and $e_x(t)$ is the difference between the measurement and the prediction obtained by the AR model. It is assumed that this difference is mainly caused by the unknown external input. Based on this assumption, a reference ARX model of the known healthy signal is constructed with the output and the difference estimated from the undamaged AR model, shown in Equation (4).

$$x(t) = \sum_{i=1}^{a} \alpha_j x(t-i) + \sum_{j=1}^{b} \beta_j e_x(t-j) + \varepsilon_x(t) \tag{4}$$

where $\varepsilon_x(t)$ denotes the residual error between the measured signal and the output of the ARX model. Finally, a new signal is fed into the reference ARX model (with the output and residual error from the "in-question" AR model as inputs), and the damage sensitive feature is obtained from the residual error. If the system experiences damage that alters the dynamic response, the reference ARX model is not able to adequately reproduce the new signal, resulting in significant variations in $\varepsilon_x(t)$. This variation will be indicated by an unusual number of residual error terms exceeding predetermined limits (called control limits). Data points outside of the limits are referred to as *outliers*. A statistically significant number of outliers indicates a system anomaly. Furthermore, the procedure

used in the AR-ARX model forces the residual error, $\varepsilon_x(t)$, to be nearly uncorrelated with no systematic pattern, if the fitted AR-ARX model is approximately correct [15], while the time signals (e.g. acceleration) are usually autocorrelated. The above brief discussion represents a primitive application of statistical pattern recognition to vibration signals that has led to documented success in the literature [1,13,14].

The features that are analyzed in the impedance methods are mainly drawn from the frequency domain. A frequency domain ARX model attempts to predict the output at a particular frequency based on the input at that frequency, as well as outputs at surrounding frequencies. The outputs at the surrounding frequencies are included as inputs to account for subharmonics and superharmonics introduced to the system through nonlinear feedback. A first order ARX model, among many possible forms of the frequency domain, is as follows [16],

$$\frac{\mathbf{Y}(\omega)}{\mathbf{U}(\omega)} \cong \mathbf{B}(\omega) + \mathbf{A}_1(\omega)\frac{\mathbf{Y}(\omega - \Delta\omega)}{\mathbf{U}(\omega)} + \mathbf{A}_{-1}(\omega)\frac{\mathbf{Y}(\omega + \Delta\omega)}{\mathbf{U}(\omega)} \tag{5}$$

where $\mathbf{Y}(\omega)$ is the response at frequency ω, $\mathbf{U}(\omega)$ is the input, and $\mathbf{Y}(\omega - \Delta\omega)$ and $\mathbf{Y}(\omega + \Delta\omega)$ are the responses at frequencies $\omega - \Delta\omega$ and $\omega + \Delta\omega$, respectively. $\mathbf{A_1}(\omega)$ and $\mathbf{A_{-1}}(\omega)$ are the frequency domain auto-regressive coefficients, and $\mathbf{B}(\omega)$ is the exogenous coefficient. These terms are then determined by minimizing the sum of the squared error associated with how well the model in Equation (5) describes the measured data. If the nonlinear terms ($\mathbf{A_1}(\omega)$, $\mathbf{A_{-1}}(\omega)$) are set to zero, the exogenous coefficient becomes equivalent to the conventional frequency response functions. More details on frequency domain analysis of data using an ARX input model can be found in the references [17, 18].

To date, impedance-based methods have focused on using the real part of the induced electrical impedance for monitoring structures. Considering the capacitive nature of the PZT, which shows the strong temperature sensitivity and manifests in the imaginary part of the impedance, only the real part is used to monitor the condition of a structure because it is dominated by structural responses. With traditional impedance analyzers, such as HP4194A, the measurement of the nonlinear terms, $\mathbf{Y}(\omega - \Delta\omega)/\mathbf{U}(\omega)$ and $\mathbf{Y}(\omega + \Delta\omega)/\mathbf{U}(\omega)$, is not currently available, imposing difficulties in using the frequency domain ARX model with the impedance methods. These nonlinear terms must be measured in the time domain and an appropriate FFT procedure is necessary. Therefore, we propose using a modified frequency domain ARX model by replacing the nonlinear terms in Equation (5) with curvatures of measured impedance data, defined as follows,

$$\frac{\mathbf{Y}(\omega)}{\mathbf{U}(\omega)} = \mathbf{B}(\omega) + \mathbf{C}_1(\omega)\frac{\partial^2}{\partial\omega^2}\left(\frac{\mathbf{Y}(\omega - \Delta\omega)}{\mathbf{U}(\omega - \Delta\omega)}\right) + \mathbf{C}_{-1}(\omega)\frac{\partial^2}{\partial\omega^2}\left(\frac{\mathbf{Y}(\omega + \Delta\omega)}{\mathbf{U}(\omega + \Delta\omega)}\right) \tag{6}$$

In Equation (6), the curvature of impedance was obtained numerically by using a central difference approximation,

$$\frac{\partial^2}{\partial\omega^2}\left(\frac{\mathbf{Y}(\omega)}{\mathbf{U}(\omega)}\right) = \frac{\partial^2}{\partial\omega^2}\left(Z(\omega)\right) = \frac{Z(\omega + \Delta\omega) - 2Z(\omega) + Z(\omega - \Delta\omega)}{(\Delta\omega)^2} \tag{7}$$

where $Z(\omega)$ is the measured impedance. It should be noted that this modified ARX model does not explicitly consider the nonlinearity as originally proposed by Adams [16]. It does not indicate strain, displacement, or velocity relationship either. Instead, by considering the coupling terms in the curvatures before and after the frequency

components, the proposed ARX model is an attempt to force the correlation of the measured impedance with the adjacent frequencies up to $\omega \pm 2\Delta\omega$, which is fine enough to allow the extraction of the unique characteristics of measured impedance data. The slope of the impedance data can also be used although the coupling terms would be limited to $\omega \pm \Delta\omega$.

Once the coefficients of $\mathbf{B}(\omega)$, $\mathbf{C}_1(\omega)$ and $\mathbf{C}_{-1}(\omega)$ are obtained with the several baseline impedance measurement in the least square sense, the model is then used to predict the response of a newly measured signal. As in the time domain AR-ARX model, this prediction model should be able to appropriately predict the new signal if the signal is close to the reference signal. On the other hand, if the new signal is recorded under a structural condition different from the conditions where reference signals were obtained, the ARX model would not reproduce the new signal adequately. Thus, the residual error is adopted as a damage sensitive feature in this method, as in the time domain analysis.

When analyzing the residual error, Extreme Value Statistics (EVS) has been employed [19, 20]. The major problem in statistical analysis is that the functional form of the distribution is often unknown and there are an infinite number of candidate distributions. However, there are only three types of distributions for the extreme (maximum or minimum) values regardless the distribution type of the parent data. Because there are only three distributions (Gumbel, Weibull, and Frechet distribution) to choose from, the distribution selection and parameter estimation becomes much easier. EVS is a powerful tool if the data of interest are in the tails (extremes) of the damage sensitive feature distribution. Control limits for the outlier analysis can be accurately

established by employing EVS from the reference impedance signals measured from the health structure. For more information on EVS, consult the reference [19,20].

In summary, the proposed damage detection algorithm consists of impedance data acquisition, construction of the frequency domain ARX model, establishment of the control limit coupled with EVS, and the statistical discrimination between features from the undamaged and damaged structures.

4. 5-Degree of Freedom System

A simulation example is presented to demonstrate the method presented above. The objective of this simulation is to perform *novelty detection* based on the outlier analysis, which identifies the existence of damage as a first step in structural health monitoring. With the impedance method, the identification of damage locations (the second step in structural health monitoring) can be easily accomplished by interrogating the PZT sensor/actuator individually employing high frequency ranges [4].

The system of interest is a simple 5 degree-of-freedom (DOF) spring-mass-damper system that has been simulated in MatLab, shown in Figure 1. Mass, damping and spring coefficients have been held constant at 7 kg, 3 N-s/m, and 7000 N/m, respectively. The system is subjected to a load at Mass 5, and the resulting response is measured at the same location. This is consistent with the *self-sensing* concept of the impedance sensors/actuators.

Changes in spring and damping coefficients of Mass 1 and Spring 1 constitute "*damage*" to the system. Damping changes has been included in this analysis, otherwise only the shifts of resonant frequency would be observed. Damage I refers to 10%

reduction in the spring, and 10% increase in the damping coefficient. Damage II refers 20% changes in both spring and damping in the same manner.

The real part of mechanical impedance was analyzed as shown in Figure 2. The deduced mechanical impedance, or mobility, is a point transfer function, hence its real part is always positive, as illustrated in Figure 2. To simulate a more realistic situation, a random noise (10% noise to signal ratio) with a Gaussian normal distribution is added to each of the undamaged and damaged response curves. With the added noise, a total of 7 undamaged responses are taken. Five of them are used to obtain the $\mathbf{B}(\omega)$, $\mathbf{C}_1(\omega)$ and $\mathbf{C}_{-1}(\omega)$ coefficients of the modified ARX model in Equation(6) and the remaining two are used for "false-positive" test.

Once the coefficients are obtained, the responses are reproduced using the ARX model. Figure 3 shows the original and reproduced mechanical impedances after fitting the ARX model under the undamaged condition. As shown in the Figure 3, the responses are very close, even with the significant noise added. In the noise-free case, the original signal was much more closely reproduced with the small errors only in the vicinity of resonant frequencies. Finally, the data from the damage conditions are measured and analyzed using the identified ARX coefficients.

Once the damage sensitive features were computed (in this case residual errors), EVS is used to accurately model the behavior of the feature distribution's tails. First, a moving window is taken along a vector of samples (measured data), and the maximum and minimum value is independently selected from each of these windows. The induced cumulative density function of these samples asymptotically converges to one of three possible distributions: Gumbel, Weibull, or Frechet, as the number of vector samples

tends to infinity. Out of three distributions, the Frechet distribution shows an accepted fit of maxima as shown in Figure 4. Thirty data points are used to estimate the distribution of tails. A nonlinear optimization problem has to be solved to estimate the distributions and associated parameters. The selection of extreme value distributions and parameter estimation is beyond the scope of this paper, and is detailed in the reference [19]. Once the acceptable distribution parameters are identified, the confidence limits are then established to assess the structural condition. These limits are far more accurate than those obtained when assuming a Gaussian distribution. The thresholds corresponding to 99.7% confidence level are calculated for both maxima and minima.

Table 1 illustrates the effectiveness of the limits found using EVS versus those calculated using the normality assumption of the data. For a sample size of 10,000 points and a 99.7% confidence interval, one should expect 15 outliers on each side of the confidence interval for undamaged data. All numbers displayed in the second row are associated with the normality assumption. Under the undamaged conditions, the confidence limits derived from EVS are much closer to the actual 99.7% limits (30 total outliers) than those derived using the normality assumption. It is clear that, if confidence limits based upon the normality assumption are used, there are many false positives, which negates any usefulness that the analysis sought. Quantitatively, there are approximately three times as many outliers as should be present with a 99.7% confidence interval, as seen in Table 1 for the baseline condition.

In damage cases, there are increasing numbers of outliers, which clearly indicates the presence of structural anomaly. The method also shows somewhat quantitative information regarding the severity of damage. With the increasing levels of damage, there

is a corresponding increase in the number of outliers. In summary, the simulation results show that the proposed damage detection algorithm coupled with EVS is able to detect damage in a structure. The method will be more effective, if it is combined with active-sensing impedance methods.

5. Proof-of-Concept Applications

The test structure, shown in Figures 5 and 6, is a simulated three-story moment-resisting frame structure, constructed of unistrut columns and aluminum floor plates. Floors are 1.3-cm-thick aluminum plates with two-bolt connections to brackets on the unistrut columns. Support brackets for the columns are bolted to this 3.8 cm think aluminum base plate. All bolted connections are tightened to a preload of 25 N-m in the undamaged state.

Four PSI-5A PZT patches (2.5 cm x 2.5 cm x 0.025 cm) are bonded to the brackets that affix the second floor to the unistrut columns for acquiring electrical impedances, as shown in Figure 7. This size makes the PZT actuators/sensors small enough not to be intrusive. The impedance measurements are made through an impedance sensing circuit in the frequency range of 5-20 kHz, as shown in Figure 8. In this circuit, V_{out} is proportional to the output current of the PZT. Electrical impedance of the PZT patch is related to the measured input and output voltage of the PZT through the following equation:

$$Z_p = \frac{V_p}{I_p} = \frac{V_{in} - V_{out}}{V_{out}/R} \Rightarrow Z_p = R \left(\frac{V_{in}}{V_{out}} - 1 \right) \tag{8}$$

A commercial data acquisition system controlled from a laptop PC is used to digitize the voltage analog signals. The Time histories are sampled at a rate of 51.2 kHz, producing 1024 frequency data points. A total of 30 averages per run is used for impedance estimates in the frequency domain. An amplified random signal (1 V) is used as the voltage input for the testing.

After measuring the several baseline impedance signatures, damage is introduced by loosening a bolt over selected locations. Two damage cases are imposed on this structure in sequence, as shown below.

- Damage I: loosening a bolt at Joint 1
- Damage II: loosening a bolt at Joint 3.

A total of 13 impedance measurements were taken over a 3-week period (7 baseline measurements, 1 measurement under Damage I, and 5 measurements under Damage II condition). The measurements were taken at different time intervals on different days. It is expected that the impedance signatures show relatively large variations because of the presence of bolted joints in the structure and slight changes in room temperature during the test. When designing and planning a long-term health monitoring system, these ambient effects should be taken into account. In the impedance-based technique, analyzing impedance signatures before and after damage would produce noticeable changes in most cases. However, a variation in the impedance measurements caused by the induced damage must be larger than that of these boundary or ambient condition changes.

The impedance measurements (real part) of PZT at joint 1 are shown in the following figures. Figure 9 shows all 7 undamaged impedance curves in the frequency

range of 5-20 kHz. The responses at 8-12 kHz are also shown for visual comparison. It can be seen that the essential pattern of the impedance signatures remains the same over the 3 week test period when damage was not induced. There are small random variations along the curves over the test period. However, the variations are relatively small and the measurements are repeatable. No noticeable degradation in the impedance signature is observed. After the damage is induced (Damage I), a significant change occurs in the signature pattern of the impedance curve over the entire frequency range, as shown in Figure 10. This is because the damage causes changes in stiffness or damping resulting in changes in mechanical impedance of the joint. All measurement readings taken after Damage II also follow a similar pattern as that of Damage I and are shown in Figure 11. Because the Joint 1 is distant from Joint 3, where Damage II is introduced, only a small change, if any, has been observed.

Both Damage I and II are well out of the sensing range of PZT bonded on Joint 2. Hence, measurements taken from this PZT do not show any significant difference from one another, as shown in Figure 12. The remaining two PZTs show the same pattern. A complete change occurs in the signature pattern of the curve over the entire frequency range when the damage is introduced close to the sensor location. If the damage is distant, there are only minor variations of the existing signature pattern.

By looking for variations in the impedance measurements, structural damage can be detected and located. However, the visual analysis of the impedance measurement graph is not suitable for on-line implementation of the impedance-based health monitoring technique. Traditionally, to simplify the interpretation of the impedance variations, a scalar damage metric is used to analyze the information from each PZT. As

described in the previous section, there are many possible damage metrics that could be used, including RMSD, cross correlation, and standard deviation. The damage metric based on RMSD is shown in Figure 13. The damage metric provides a summary of the information obtained from the impedance response curves.

As can be seen in Figure 13, there is an increase in damage metric if damage is located close to the PZT. Normal variations are relatively small. It should be noted that, because of relatively low frequency range being used in this study (5-20 kHz) as compared to traditional impedance approaches (> 30 kHz), it is expected that damage initiated at one joint can be picked up by sensors at the other joints. In addition, because of the relatively small dimension of the structure, it is visually observed that the structure undergoes somewhat global changes with the induced damage, i.e., twisting and/or bending of the aluminum floor plate and joints, making damage localization quite difficult.

The other damage metrics using cross correlation or standard deviation follow the similar pattern as those shown in Figure 13. However, none of these methods establishes threshold values or statistical confidence on the structure condition. The decision-making is somewhat arbitrary and there is currently no rigorous statistical method implemented into the impedance method.

In order to apply the proposed outlier analysis, the first five baseline measurements are used to obtain auto-regressive coefficients and exogenous coefficients of the modified ARX model. Once the coefficients are identified, the residual errors are extracted as a damage sensitive feature by substracting the measured impedance and predicted output of the ARX model. Once again, EVS is employed to establish the

confidence limit of 99.5%, and it is determined that the Frechet distribution is the most appropriate extreme value distribution for the use in the analysis. If the normality assumption is used, there would be many false positives with the inflated number of outliers. The selection of the decision limit depends on the specific structure and type of damage to be monitored. The 99.5% is chosen in this study because it provides acceptable risk. For a sample size of 1020 points and a 99.5% confidence interval, 5 or 6 outliers beyond the confidence interval for an undamaged case are expected.

Figures 14 and 15 show the residual errors as well as the associated 99.5% confidence interval, for Joint 1. Figure 14 depicts the baseline undamaged case and Figure 15 shows Damage case I, in which Joint 1 has been damaged. There is a clear visual distinction between the undamaged and damaged conditions.

The number of outliers for each joint and for each damage case is shown in Figure 16. It can be seen that results from the undamaged condition, tests 1 through 7, are excellent, showing no false positive indication of damage at all joints. Two damage conditions are then correctly identified. At damage I, there is a large increase in the number of outliers (38) at Joint 1, which is clearly indicative of damage at the location. PZT 3 does not show any changes, compared to the baselines and compared to PZTs 2 and 4, because it is located farthest away (diagonally apart) from the damaged joint. When Damage II was introduced, there was a large increase in the number of outliers (39) at the newly damaged joint, and a small increase in the number of outliers at Joints 2 and 4. This result shows that the proposed algorithm coupled with impedance methods can clearly detect and locate a state of structural damage.

The proposed method provides a distinct advantage to traditional impedance-based health monitoring approaches. The inclusion of a rigorous statistical framework enables a more quantitative assessment of the damaged and undamaged conditions. As stated, the main limitation of previous impedance-based approaches was "how to establish appropriate control limit or thresholds values for damage indication." The decision was typically made based on arbitrary values, i.e., "small variations" for undamaged cases and "large variations" for damaged cases. In this proposed approach, the undamaged condition can be quantitatively assessed by tracking the number of outliers. The numbers within or below the control limit can be considered as an undamaged state. In the case of damage present, the proposed algorithm shows a statistically significant number of outliers outside the control limits that allows a diagnosis of the damage state in a more conclusive manner.

The identified outliners can also be considered as "key indicators" for damage identification and structural health monitoring. For real-world applications, the impedance measurement would produce overwhelming amounts of data from hundreds of sensors. Data compression into a small dimensional feature is required by this constraint. The proposed algorithm allows the condensation of the large amount of data into a much smaller data set, allowing automated health monitoring without human interaction.

6. Discussions

A statistical pattern recognition algorithm has been incorporated into the impedance-based structural health monitoring technique. The results collected from the numerical and experimental tests demonstrated the capability of this technology to detect

damage in a statistically quantifiable manner. There are, however, certain research issues remaining for more effective implementation of the proposed technique.

The robustness of the proposed algorithm against ambient condition changes, such as significant temperature variations, should be investigated and improved. In addition to the residual errors used in this study, different parameters, such as relative and/or absolute changes in exogenous or autoregressive ARX coefficients can also be used as damage sensitive features and may provide a better performance in damage identification.

It has been found that the frequency domain ARX coefficients are sensitive to leakage [16] in the frequency response measurements. In this study, a prior curve fitting on the impedance data was performed before constructing the ARX model in order to minimize this effect. In addition, the effects of measurement noises on the proposed algorithm should be thoroughly investigated. The feature extraction in this method involves the process of differentiating a frequency domain spectrum as a function of frequency using a central difference curvature expansion. This differentiation often leads to amplifications of existing noise in data. Therefore, a study is needed to identify and quantify the effects of leakage and noise in experimental data on the proposed algorithm.

The inclusion of EVS improves the reliability of the method by placing it within a rigorous statistical framework. However, the selection of proper EVS distribution for each data set and the evaluation of associated distribution parameters are still heavily based on an initial guess and a trial-and-error method. A new process that automates estimation of proper distributions and associated parameters needs to be established.

These issues are currently under investigation and the results will be published in the near future.

7. Conclusion

A new pattern recognition approach that capitalizes the features of impedance signals has been presented for structural damage identification problems. A modified auto-regressive model with exogenous inputs in the frequency domain is developed, and associated prediction errors are used as damage sensitive features. The method of outlier analysis is then adopted to determine the damage state of a structure. Furthermore, extreme value statistics is used to establish proper confidence limits because of the non-Gaussian nature of the identified feature distribution tails. A numerical example on a 5 degree of freedom system and experimental results on a three-story building model have been presented to demonstrate the proposed concept. It has been found that the proposed algorithm could assess the condition of a structure in a more quantifiable manner over the traditional impedance approaches.

ACKNOWLEDGMENTS

Funding for this project was provided by the Department of Energy through the internal funding program (LDRD-DR) at Los Alamos National Laboratory, entitled “Damage Prognosis Solution.”

REFERENCES

[1] H. Sohn, C.R. Farrar, Damage Diagnosis using Time Series Analysis of Vibration Signals, *Smart Materials and Structures*, 10 (2001), 446-451.

[2] C.R. Farrar, T.A. Duffey, S.W. Doebling, D.A. Nix, A Statistical Pattern Recognition Paradigm for Vibration-based Structural Health Monitoring, *Proceedings of 2nd International Workshop on Structural Health Monitoring*, Stanford, CA, 2000, 764-773.

[3] G. Park, H.H. Cudney, D.J. Inman, Impedance-based Health Monitoring of Civil Structural Components, *ASCE Journal of Infrastructure Systems*, 6 (2000), 153-160.

[4] G. Park, H. Sohn, C.R. Farrar, D.J. Inman, Overview of Piezoelectric impedance-based health monitoring and Path Forward, *The Shock and Vibration Digest,* 35 (2003), 451-463.

[5] C. Liang, F.P. Sun, C.A. Rogers, Coupled Electro-Mechanical Analysis of Adaptive Material Systems-Determination of the Actuator Power Consumption and System Energy Transfer, *Journal of Intelligent Material Systems and Structures*, 5 (1994), 12-20.

[6] J.P. Stokes, G.L. Cloud, The Application of Interferometric Techniques to the Nondestructive Inspection of Fiber-reinforced Materials, *Experimental Mechanics*, 33(1993), 314-319

[7] F.P. Sun, C.A. Roger, C. Liang, Structural Frequency Response Function Acquisition via Electric Impedance Measurement of Surface-Bonded Piezoelectric Sensor/Actuator, *Proceedings of 36th AIAA/ASME/ASCE/AHS/ASC Structures, Structural Dynamics, and Materials Conference*, 1995, 3450-3461.

[8] F.P. Sun, Z. Chaudhry, C. Liang, C.A. Rogers, Truss Structure Integrity Identification Using PZT Sensor-Actuator, *Journal of Intelligent Material Systems and Structures*, 6 (1995), 134-139.

[9] V. Raju, G. Park, H.H. Cudney, Impedance-based Health Monitoring Technique of Composite Reinforced Structures, *Proceedings of 9th International Conference on Adaptive Structures and Technologies*, Cambridge, MA, 1998, 448-457

[10] A.N. Zagrai, V. Giurgiutiu, Electro-Mechanical Impedance Method for Crack Detection in Thin Plates, *Journal of Intelligent Material Systems and Structures*, 12 (2001), 709-718.

[11] D.C. Montgomery, *Introduction to Statistical Quality Control, Third Edition*, John Wiley & Sons, Inc. ISBN 0-471-30353-4, 1997.

[12] G.E.P. Box, G.M. Jenkins, G.C. Reinsel, G.C., *Time SeriesAnalysis: Forecasting and Control* 3rd ed. (Englewood Cliffs, NJ: Prentice-Hall), 1994

[13] K. Worden, G. Manson, N.R.J. Fieller, Damage Detection using Outlier Analysis, *Journal of Sound and Vibration*, 229 (2000), 647-667

[14] H. Sohn, C.R. Farrar, N.F. Hunter, K. Worden, Structural Health Monitoring Using Statistical Pattern Recognition Techniques, *ASME Journal of Dynamic Systems, Measurement and Control: Special Issue on Identification of Mechanical Systems*, 123 (2001), 706-711.

[15] M.L. Fugate, H. Sohn, C.R. Farrar, Vibration-based Damage Detection using Statistical Process Control, *Mechanical Systems and Signal Processing*, 15 (2001), 707-721

[16] D.E. Adams, Frequency Domain ARX Models and Multi-Harmonic FRF Estimators for Nonlinear Dynamic Systems, *Journal of Sound and Vibration*, 250 (2001)**,** 935-950.

[17] D.E. Adams, R.J. Allemang, Discrete Frequency Models: A New Approach to Temporal Analysis, *ASME Journal of Vibration and Acoustics* 123 (2000), 98-103.

[18] D.E. Adams, C.R. Farrar, Identifying Linear and Nonlinear Damage Using Frequency Domain ARX Models, *International Journal of Structural Health Monitoring* 1 (2002), 185-201.

[19] E. Castillo *Extreme Value Theory in Engineering*; Academic Press Series in Statistical Modeling and Decision Science: San Diego, CA, 1988.

[20] H. Sohn, D.W. Allen, K. Worden, C.R. Farrar, (2003) "Structural Damage Classification Using Extreme Value Statistics," *ASME Journal of Dynamic Systems, Measurement, and Control*, in press.

LIST OF FIGURES

LIST OF TABLES

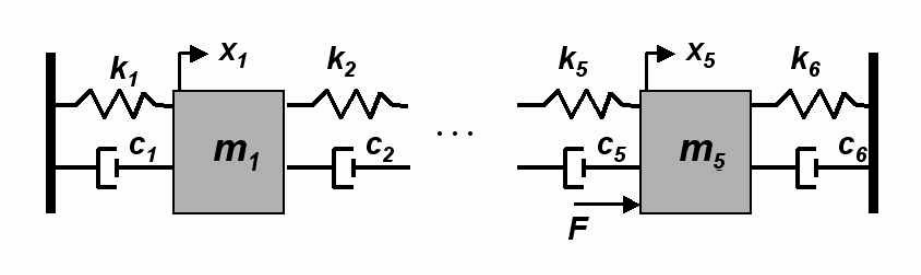

Figure 1: Conceptual drawing of the 5 DOF system

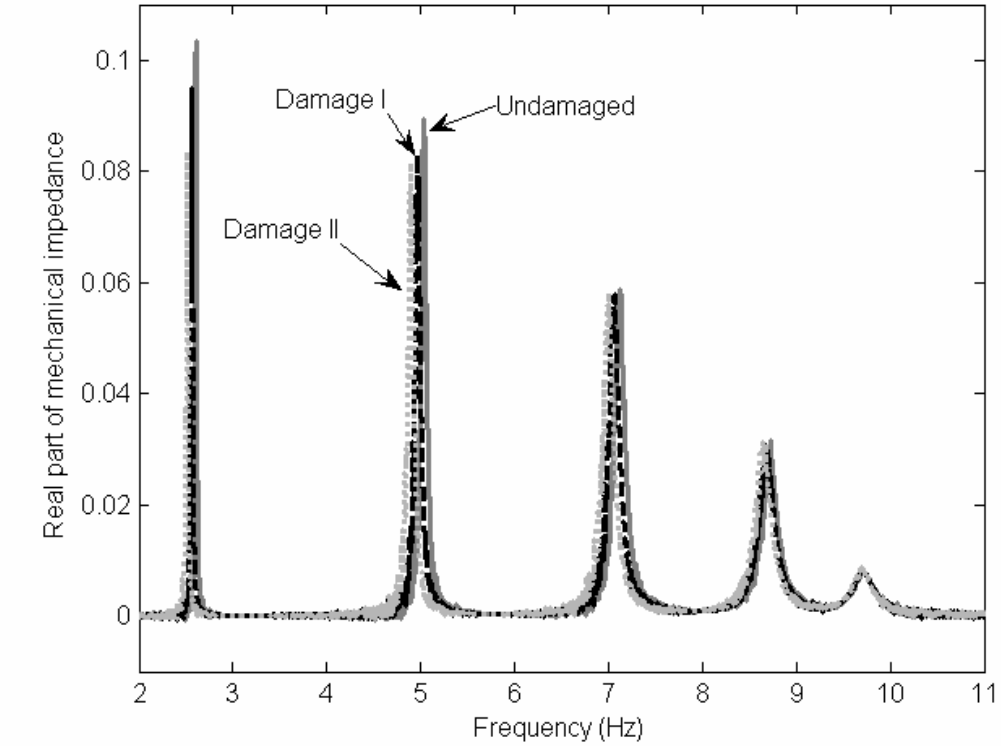

Figure 2: Real part of mechanical impedance with Gaussian noise added: solid line, Undamaged; dashed line, Damage I; dotted line, Damage II **.**

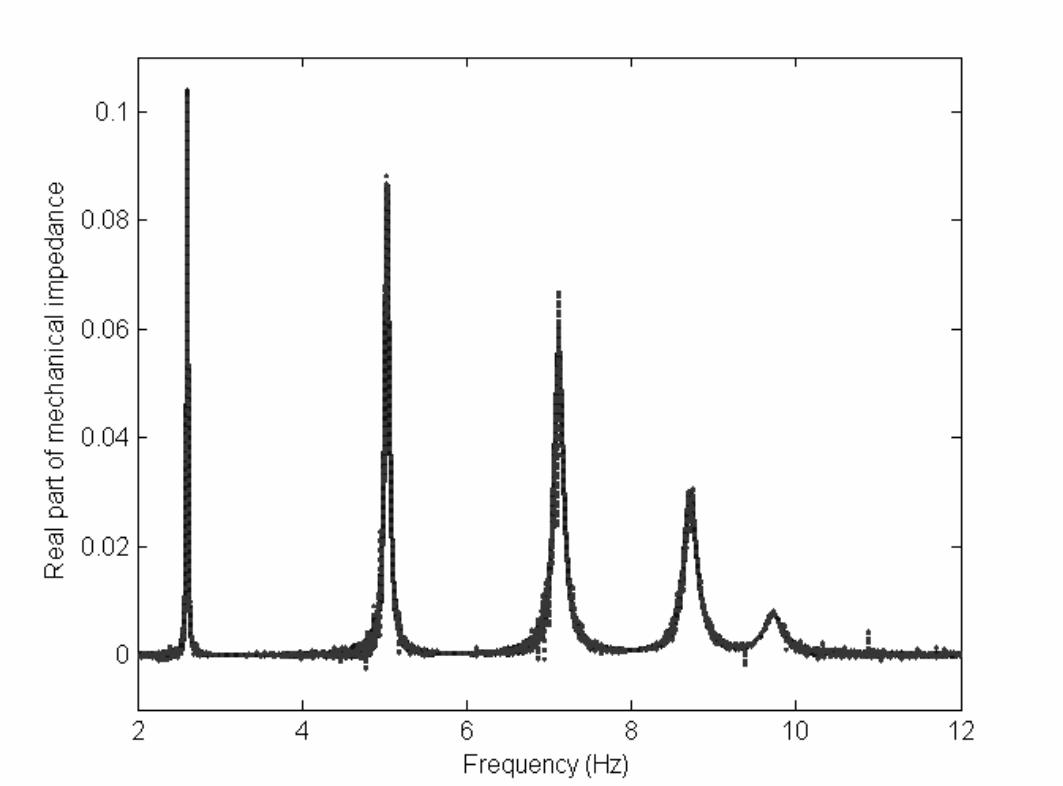

Figure 3: Original and regenerate signals after fitting the ARX model: solid line, Original Signal; dotted line, Regenerated signal

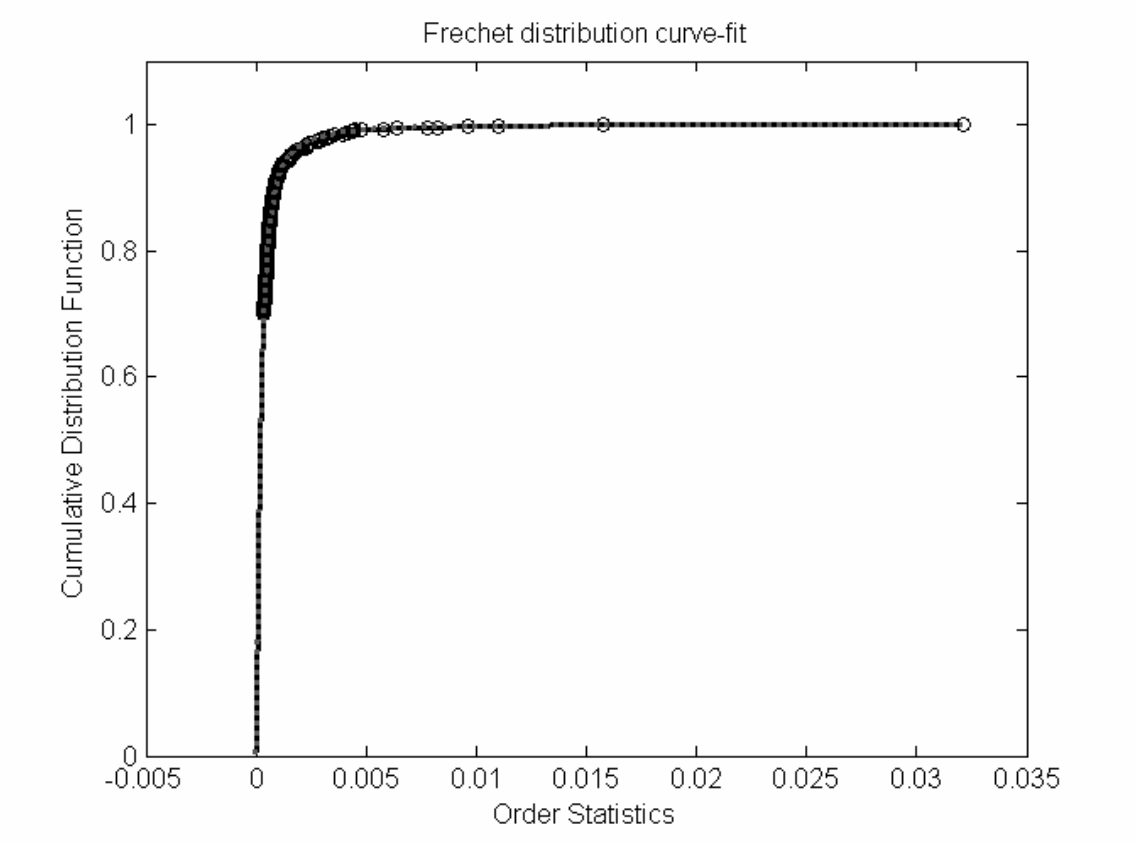

Figure 4: Curve fit for Frechet maxima distribution: solid line, Empirical CDF; o, Points used; dotted line, Fitted CDF

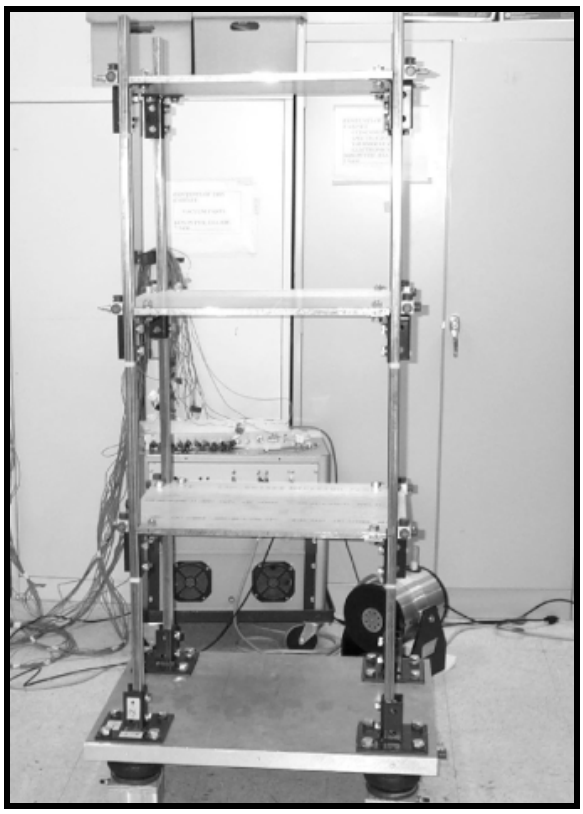

Figure 5: Assembled moment-resisting frame test structure

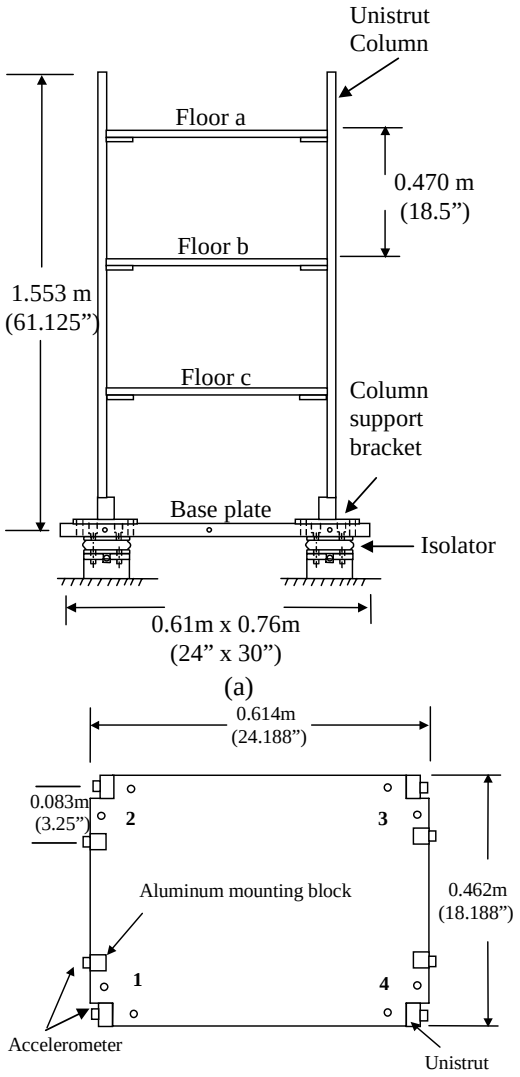

Figure 6: A schematic of the test structure: (a) Side view; (b) Top view

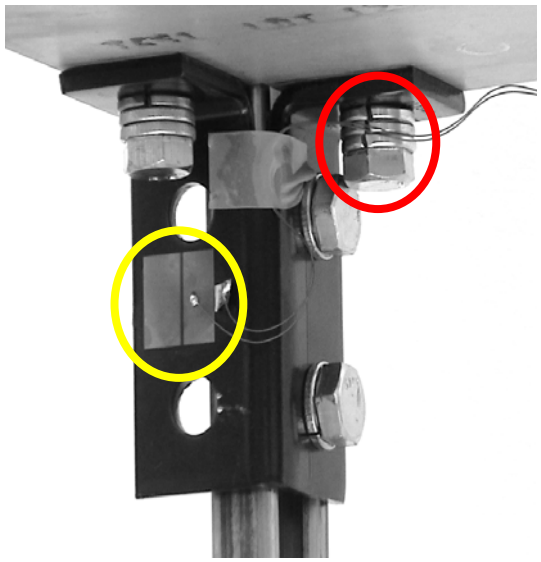

Figure 7: Close-up of joint with bonded PZT patch (light circle) and loosened bolt in damage case (dark circle)

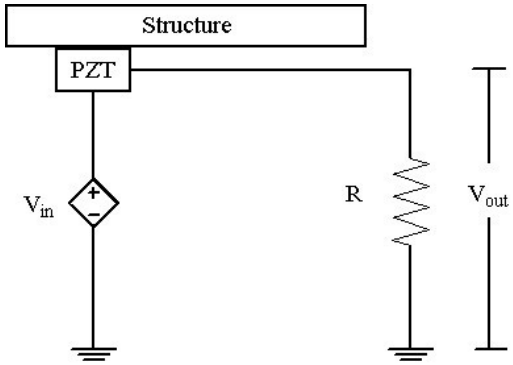

Figure 8: Diagram of PZT circuit indicating locations of measured voltages V_{in} and V_{out}

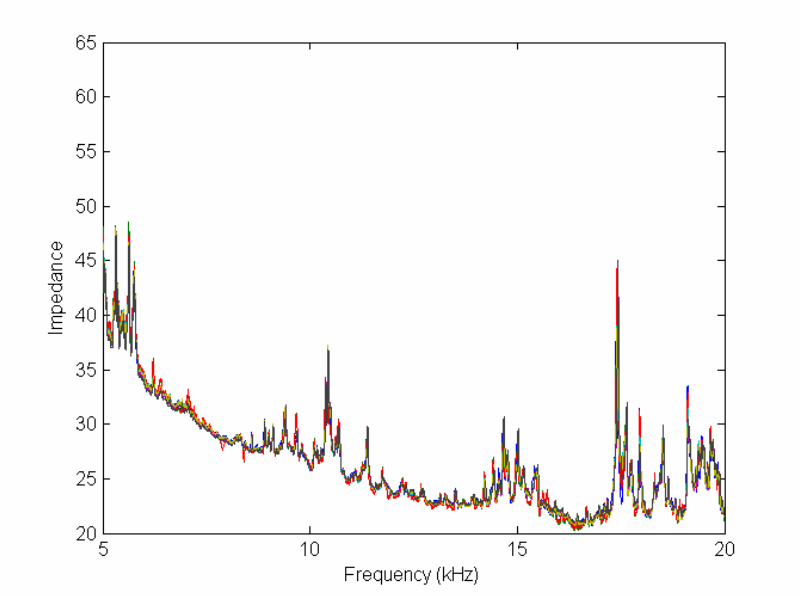

(a)

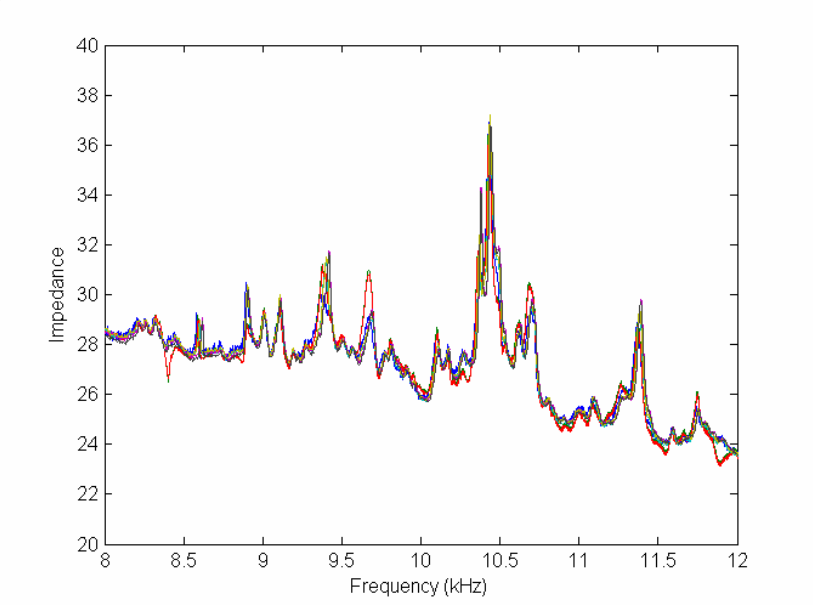

(b)

Figure 9: Seven baseline impedance measurements at Joint 1 before damage was introduced: (a) 5-20 kHz; (b) 8-12 kHz.

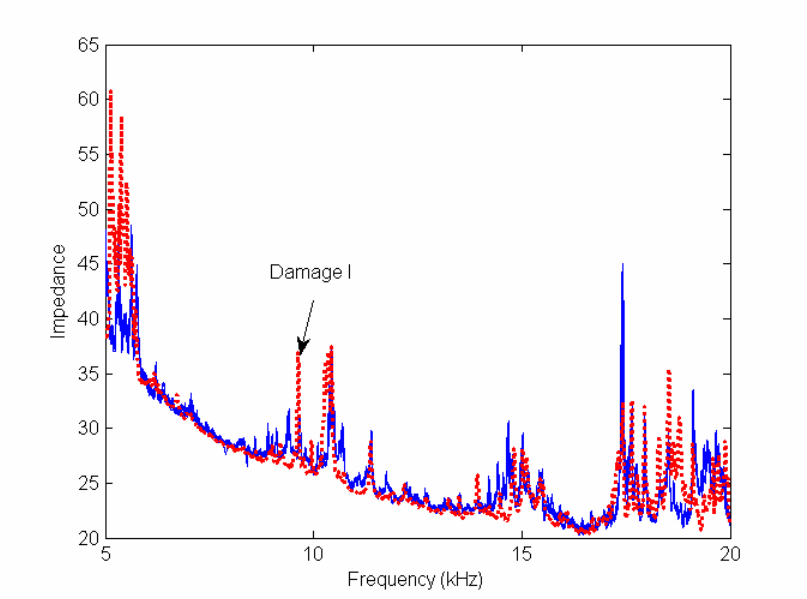

(a)

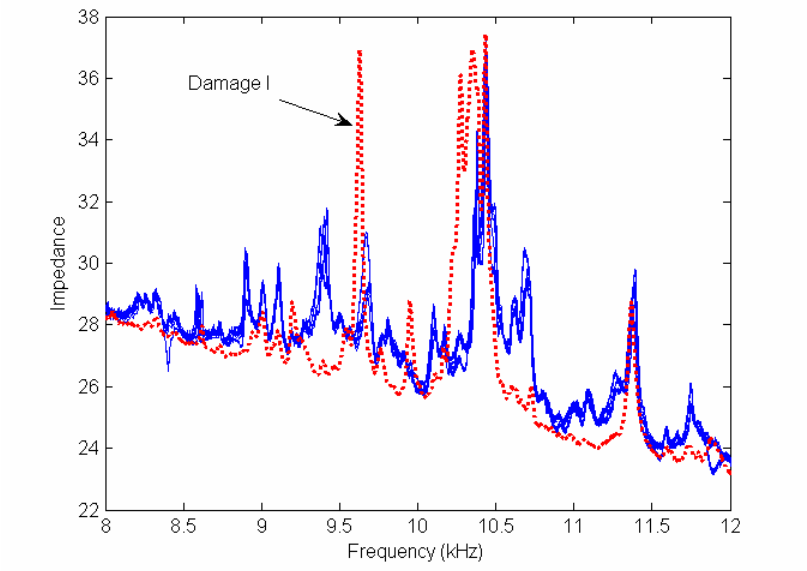

(b)

Figure 10: A significant change has been observed with the induced damage (Joint 1) : (a) 5-20 kHz; (b) 8-12 kHz.: solid line, undamaged; dotted line, damaged

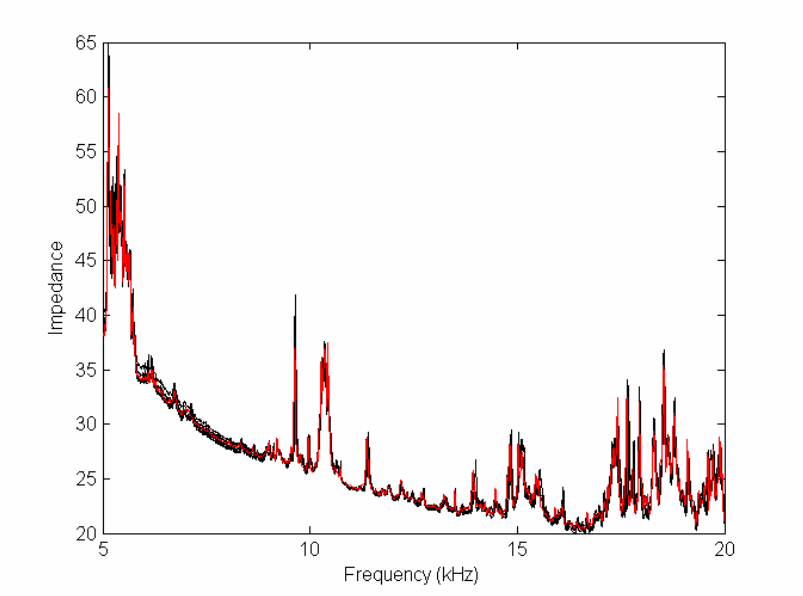

(a)

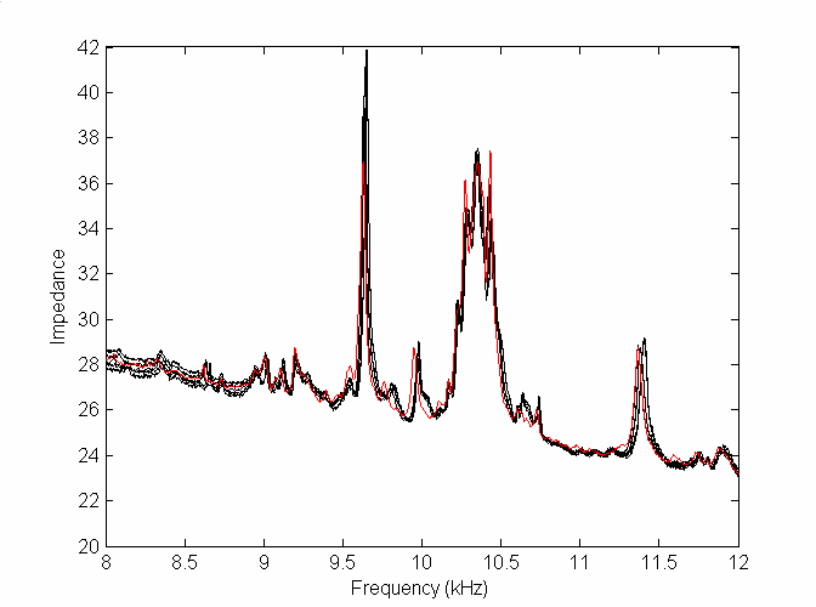

(b)

Figure 11: Impedance measurements at Joint 1 under Damage I and Damage II condition. (Joint 1): (a) 5-20 kHz; (b) 8-12 kHz.

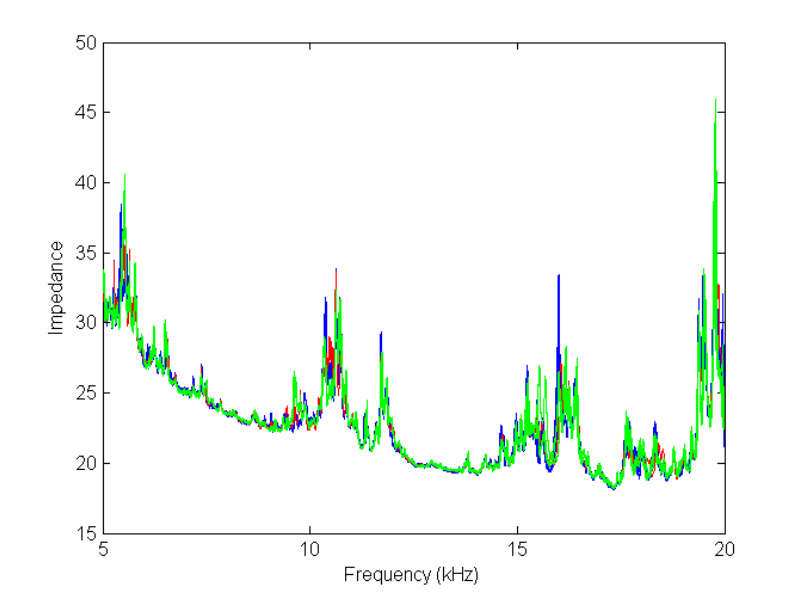

Figure 12: Impedance measurements at Joint 2 throughout the test, before and after damage I and II

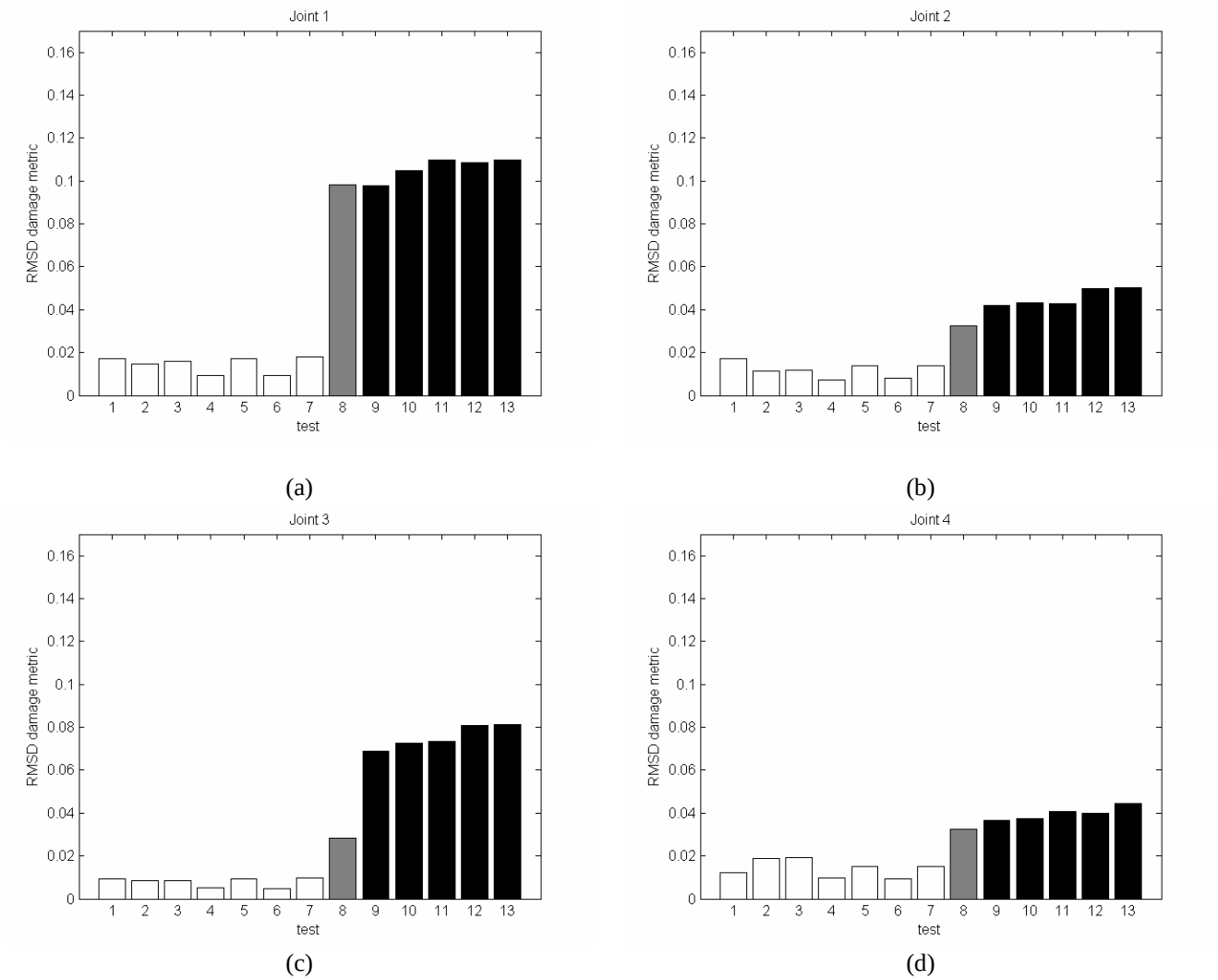

Figure 13: RMSD damage metric: (a) Joint 1; (b) Joint 2; (c) Joint 3; (d) Joint 4: undamaged, white; Damage 1 (Joint 1), gray; Damage II (Joint 3), black

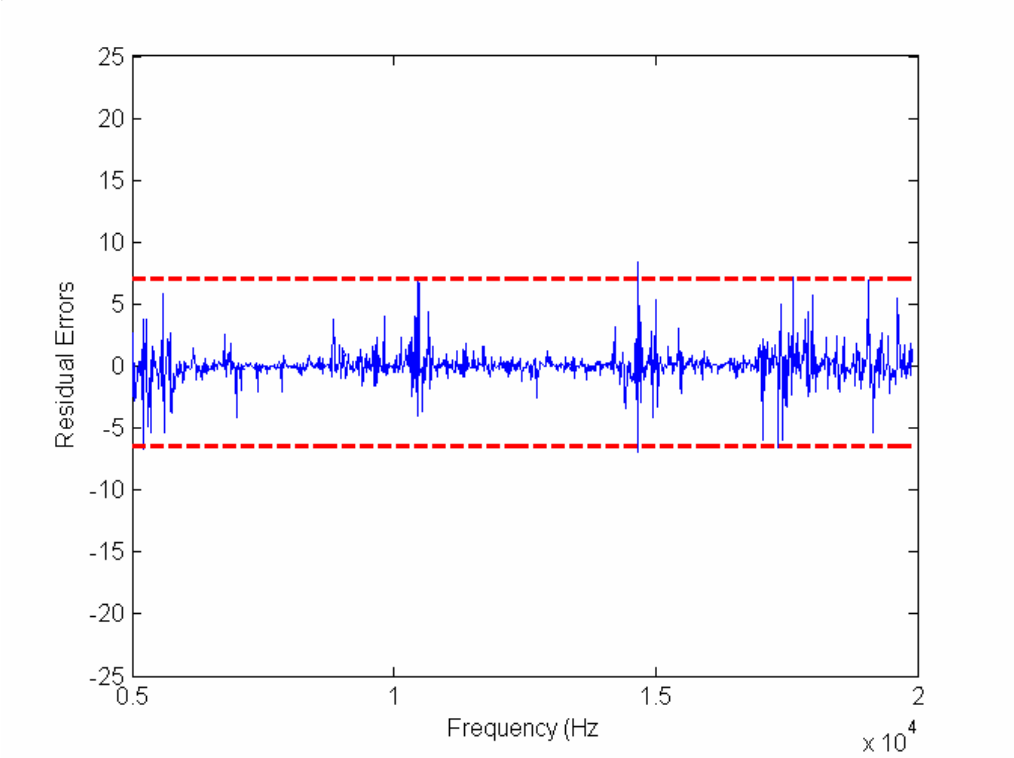

Figure 14: 99.5% confidence interval of baseline undamaged case for Joint 1

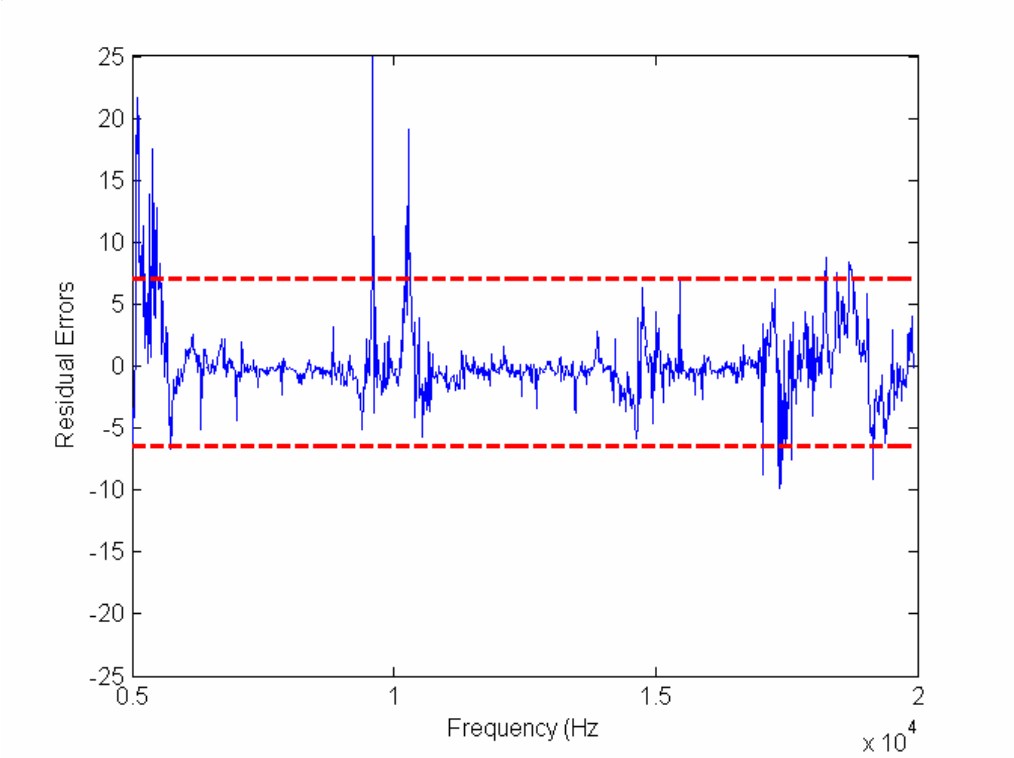

Figure 15: 99.5% confidence interval of baseline damaged case for Joint 1

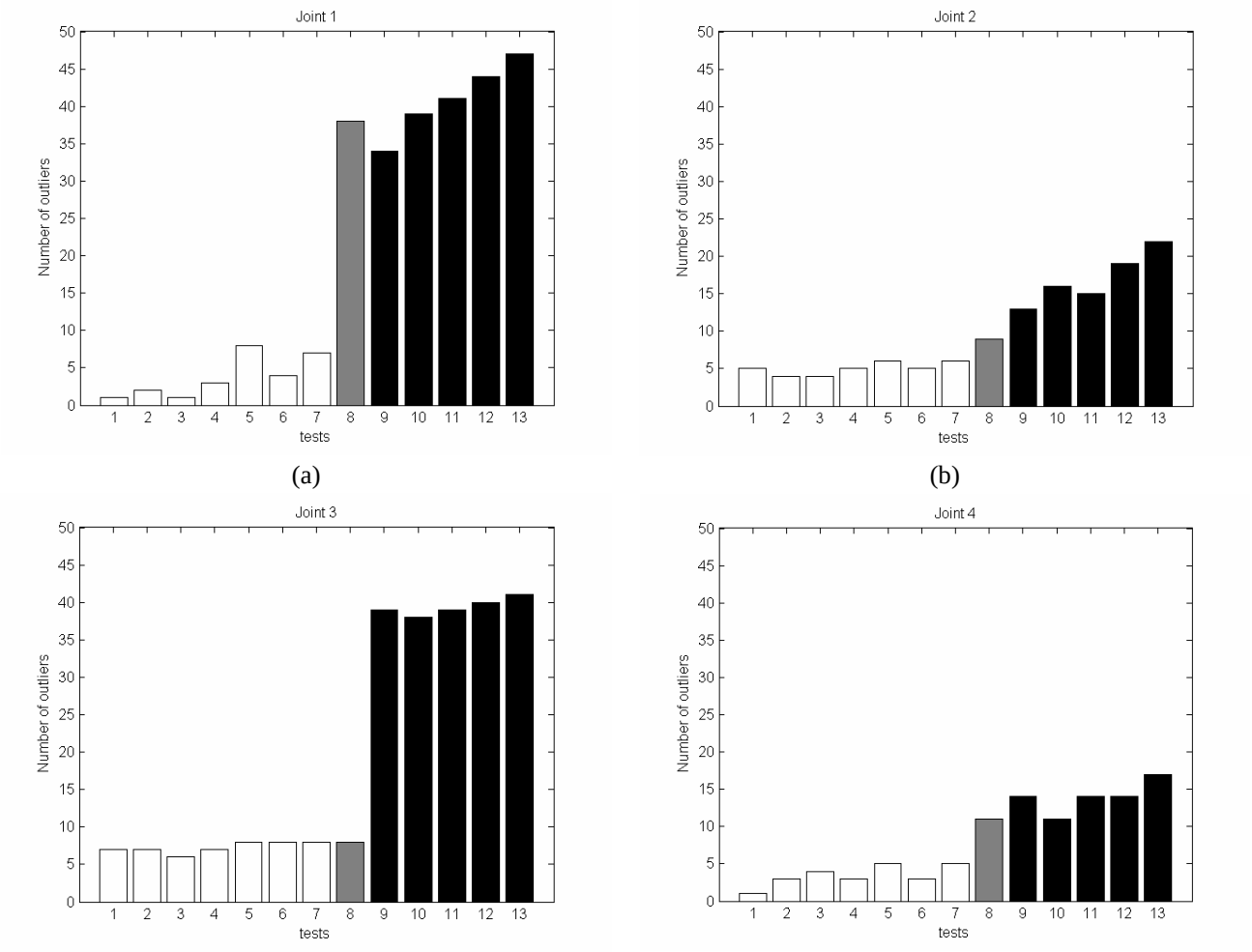

Figure 16: Total number of outliers using EVS confidence limits for each joint: (a) Joint 1; (b) Joint 2; (c) Joint 3; (d) Joint 4: undamaged, white; Damage 1 (Joint 1), gray; Damage II (Joint 3), black

Outliers	**Undamaged**							**Damaged**	
	1	**2**	**3**	**4**	**5**	**6**	**7**	**I**	**II**
EVS	28	26	25	23	28	37	32	573	824
Gaussian	129	100	107	100	107	161	155	898	1173

Table 1: Total number of outliers using EVS and Gaussian confidence limits